ACS Catalysis

Research Article

pubs.acs.org/acscatalysis

$MnCo_2O_4$ Anchored on P-Doped Hierarchical Porous Carbon as an Electrocatalyst for High-Performance Rechargeable Li–O_2 Batteries

Xuecheng Cao,[†] Jiao Wu,[†] Chao Jin,[†] Jinghua Tian,[†] Peter Strasser,[‡] and Ruizhi Yang*[,†]

[†]College of Physics, Optoelectronics and Energy & Collaborative Innovation Center of Suzhou Nano Science and Technology, Soochow University, Suzhou, Jiangsu 215006, China

[‡]Department of Chemistry, Chemical Engineering Division, Technical University Berlin, 10623 Berlin, Germany

Supporting Information

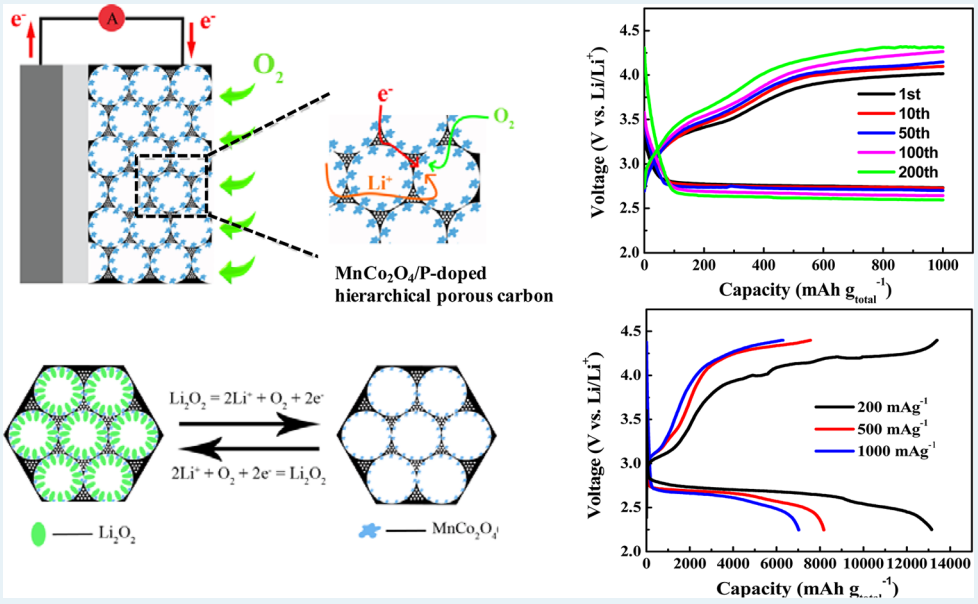

ABSTRACT: The design and synthesis of $MnCo_2O_4$ anchored on P-doped hierarchical porous carbon (MCO/P-HPC) is reported. Without harsh oxidative treatment, creating anchoring sites for $MnCo_2O_4$ on the surface of carbon is realized by P-doping in carbon. The chemical coupling between P-HPC and MCO induced by P-doping provides pathways for fast charge transport. This hybrid with a hierarchical porous structure favors efficient electrolyte penetration, oxygen transport, and effective accommodation of insoluble discharge product Li_2O_2. When employed as an electrocatalyst in rechargeable Li–O_2 batteries, the MCO/P-HPC hybrid delivers a high discharge capacity (13 150 mAh g^{-1} at 200 mA g^{-1}), excellent rate capability (7028 mAh g^{-1} at 1000 mA g^{-1}), and long cycle stability (200 cycles at a capacity of 1000 mAh g^{-1} under 200 mA g^{-1}).

KEYWORDS: *Li–O_2 battery, electrocatalyst, $MnCo_2O_4$, P-doped carbon, chemical coupling*

INTRODUCTION

The rechargeable nonaqueous Li–O_2 batteries have attracted a great deal of attention because of their high theoretical energy density (11 680 Wh kg^{1-}), which is more than 10 times that of the current commercial Li-ion batteries,[1−5] and can meet the high energy density requirement for electric vehicles and electrical energy storage for grid. However, low round-trip efficiency, low charge/discharge rate, and poor cyclability limit the practical application of Li–O_2 batteries. Great challenges exist in air electrode. The oxygen reduction reaction (ORR) and oxygen evolution reaction (OER) at the air electrode during discharge and charge are sluggish, which require efficient electrocatalysts to accelerate their rates. Meanwhile, the insoluble discharge products (Li_2O_2) can block the pores of air electrode and hinder the transport of electrolyte and oxygen during charge/discharge process.[6,7] Therefore, developing highly efficient catalysts and rationally designing air electrodes are challenging with respect to Li–O_2 batteries.[6−9]

Spinel oxides have been investigated as efficient low-cost catalysts for the air cathode of Li–air batteries.[10−12] In particular, $MnCo_2O_4$ spinel oxide, with Co and Mn having multiple valence state, affords promising electrocatalytic activity for ORR and OER. However, the poor electronic conductivity limits the catalytic activity of spinel oxides.[13,14] The most

Received: March 9, 2015
Revised: July 3, 2015
Published: July 9, 2015

DOI: 10.1021/acscatal.5b00494
ACS Catal. 2015, 5, 4890−4896

Scheme 1. Schematic Illustration of the Preparation of $MnCo_2O_4$/P-Doped Hierarchical Porous Carbon (MCO/P-HPC) (a) and the Structure of a Li−O_2 Battery (b)

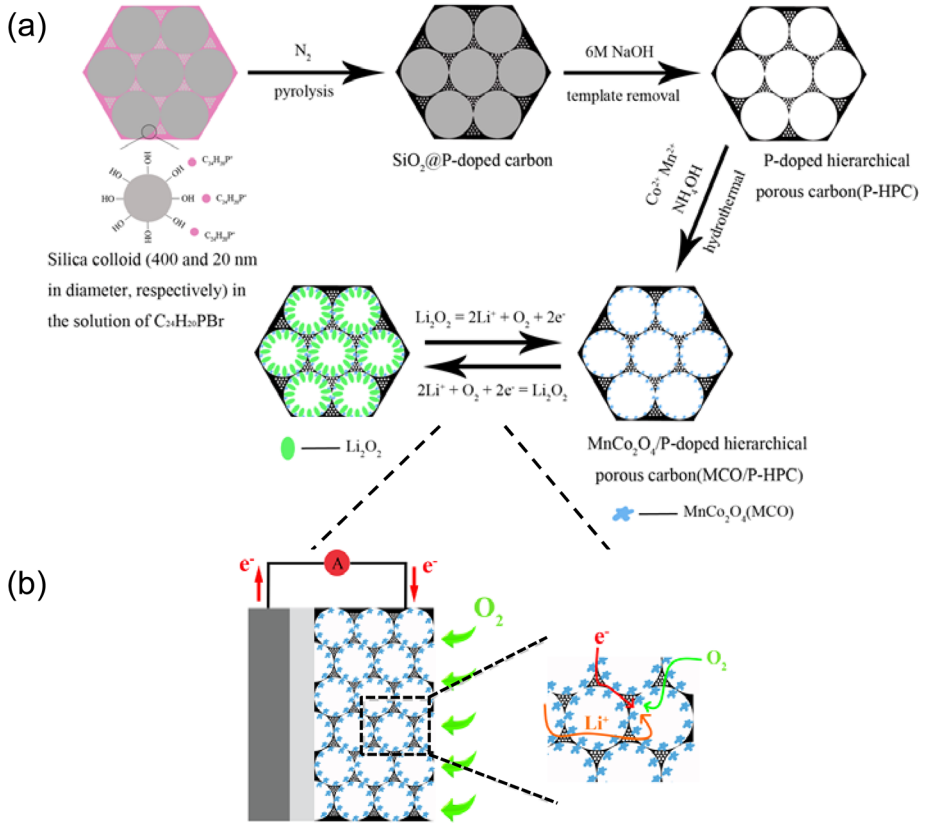

common strategies to solve this problem are to support spinel oxides onto a conductive carbon substrate. On the basis of their strongly coupled hybrid approach, Dai and co-workers prepared $MnCo_2O_4$/ graphene hybrid, which delivered a capacity of ~3784 mAh g^{-1} at a current density of 100 mA g^{-1} when used as a cathode electrocatalyst for rechargeable Li−O_2 batteries.[12] As is well-known, to ensure an intimate contact between metal oxide and carbon substrate, carbon is usually pretreated with harsh oxidative agents to have sufficient functional groups to coordinate the metal ions. However, excessive oxidation of carbon will inevitably destroy the sp^2 structure of carbon and therefore decrease the electronic conductivity of carbon. This requires the oxidation degree of carbon to be carefully controlled to balance the surface functional groups and the electronic conductivity of carbon.[15] This makes the process control of metal oxide/carbon hybrid complicated. Therefore, other method for functionalizing the surface of carbon for anchoring metal oxides needs to be explored. Recently, phosphorus (P) doping has been reported to be an effective way to improve the electronic conductivity of carbon. Moreover, P doping induces not only structural changes of carbon (like high plane edge exposure) but also charge redistribution of carbon, creating charge sites of C^-.[16−19] Therefore, it can be expected that doping of P in carbon could provide nucleation sites for metal oxides while improving the electronic conductivity of carbon.

To further boost the performance of Li−O_2 batteries, the morphology of electrocatalysts is considered to be important for the air electrode design. Specifically, the hierarchical porous structure not only facilitates the electrolyte immersion, electron and Li^+ transport but also provides an effective space for O_2 diffusion and O_2/Li_2O_2 conversion,[20−25] which are beneficial for the rate capability and cycling capability of the Li−O_2 batteries.

Herein, we design and construct a hybrid of $MnCo_2O_4$ and P-doped hierarchical porous carbon (MCO/P-HPC) for the first time. P-doped hierarchical porous carbon is first synthesized using a template method coupled with an electrostatic attraction process. Then $MnCo_2O_4$ is supported on the as-synthesized P-doped hierarchical porous carbon with a hydrothermal method. Without harsh oxidative treatment, creating anchoring sites for $MnCo_2O_4$ on the surface of carbon is realized by P-doping in carbon. Meanwhile the chemical coupling forms between $MnCo_2O_4$ and P-doped carbon. This MCO/P-HPC hybrid favors the transport of electron, Li^+ as well as O_2, and also effectively accommodates insoluble discharge product Li_2O_2 (Scheme 1). With this MCO/P-HPC hybrid catalyst, the Li−O_2 battery exhibits a high specific capacity, excellent rate capability and cycling performance.

EXPERIMENTAL SECTION

Sample Preparation. *Synthesis of SiO_2 Templates.*

(1) SiO_2 with a diameter of 400 nm, 14.7 mL of ultrapure water, 65 mL of alcohol, and 80 mL of $NH_3{\cdot}H_2O$ were mixed to be a transparent solution. Subsequently, 6.94 mL of tetraethyl orthosilicate (TEOS) was added into the mixture followed by continuous stirring for 4 h. Then the precipitate was collected and washed with water and alcohol for several times. The obtained white powder was dried at 60 °C for at least 24 h.

(2) SiO_2 with a diameter of 20 nm, 139 g of ultrapure water, 10.88 g of $C_{12}H_{26}$, and 0.146 g of lysine were mixed, and

DOI: 10.1021/acscatal.5b00494
ACS Catal. 2015, 5, 4890−4896

11.51 mL of TEOS was added to the mixture followed by continuous stirring for 20 h at 60 °C. Then the mixture was kept static at 100 °C for another 20 h. Finally, the mixture was dried at 100 °C, and the obtained powder was annealed at 600 °C for 3 h to remove the organic component.

Synthesis of P-Doped Hierarchical Carbon (P-HPC). Initially, 1.2 g of $C_{24}H_{20}PBr$ was added into 25 mL of ethanol to form a transparent solution. One gram of SiO_2 with a diameter of 400 nm, 0.1 g of SiO_2 with a diameter of 20 nm, and 5 mL of ultrapure water were added, and the mixture was stirred for 2 h. Then the mixture was dried with a slow rate at 45 °C. The obtained white powder was annealed at 800 °C for 2 h under an inert atmosphere. Then 6 M NaOH solution was used to remove SiO_2 templates.

Synthesis of $MnCo_2O_4$ Anchored on P-Doped Hierarchical Carbon Hybrid (MCO/P-HPC). In the firs step, 12.62 mg of $C_4H_6CoO_4{\cdot}4H_2O$ and 6.21 mg of $C_4H_6MnO_4{\cdot}4H_2O$ were added into 17 mL of alcohol to form a pink solution. Ten milligrams of as-obtained P-HPC, 0.5 mL of ultrapure water, and 0.5 mL of $NH_3{\cdot}H_2O$ were added, and the mixture was stirred for 10 h at 80 °C. Then the mixture was transferred to an autoclave and kept at 150 °C for 3 h. After washing and drying, the MCO/P-HPC catalyst was obtained.

The synthesis of free MCO is similar to that of MCO/P-HPC only without adding P-HPC.

Electrochemical Measurements. The MCO/P-HPC (MCO or P-HPC), conductive carbon (acetylene black), and PVDF were mixed with a mass ratio of 45:45:10. *N*-methyl-2-pyrrolidone (NMP) was added to make the mixture well-dispersed. The resulting dispersion was sprayed onto carbon paper which was used as a current collector. The mass loading of each air electrode is about 0.13 mg cm^{-2}. The electrolyte was 1 M lithium bis(trifluoromethane sulfonimide) (LiTFSI) in tetraethylene glycol dimethyl ether (TEGDME). The Li−O_2 battery was assembled using a 2032-type coin cell, which includes a lithium metal anode(Ø =15 mm), a glass-fiber separator(GFC, Whatman, Ø=19 mm) impregnated with electrolyte, and a well-prepared air electrode (Ø =14 mm). The assembling of a Li−O_2 battery was conducted in a glovebox filled with Ar. The electrochemical tests of batteries were conducted in another glovebox filled with Ar/O_2 (molar ratio of 4:1). The Li−O_2 batteries were tested on a LAND BT2000 battery test system (WuHan, P.R. China). All the tests were performed in the range between 2.2 and 4.4 V.

Physical Characterization. The XRD patterns of the samples were collected on a Bede D1 X−ray diffractometer (U.K., Bede Scientific Ltd.; Cu Kα radiation, λ = 0.15418 nm; operated at 40 kV, 45 mA). For the measurements on the discharged−charged electrodes, the electrodes were washed with TEGDME and dried under vacuum to remove the residual solvent. Then the electrode was transferred to a sample holder sealed with Kapton film.

The morphology of catalysts was examined on a scanning electron microscopy (SEM, FEI Quanta 200).

The microstructure of the samples was characterized by a transmission electron microscope (TEM,TecnaiG220) operating at 200 kV.

The specific surface area and the pore structure of the samples were analyzed by adsorption/desorption measurements of nitrogen at 77 K (TriStar II3020). Surface area and pore size distribution were calculated by Brunauer−Emmett−Teller (BET) and Barrett−Joyner−Halenda (BJH) method, respectively.

The elements binding environment of the samples was analyzed with a X-ray photoelectron spectroscopy spectrometer (XPS, VG ESCALAB MKII). The spectra were corrected for the background using the Shirley approach. The surface content of P in P-HPC was calculated from the XPS data.

The amount of $MnCo_2O_4$ in the MCO/P-HPC hybrid was determined by thermogravimetric analysis (TGA, PerkinElmer TGA7, air: 40−800 °C, heating rate: 5 °C min^{-1}), which was calibrated with calcium oxalate. The bulk content of P in the carbon was measured with inductively coupled plasma-atomic emission spectroscopy (ICP-AES) analysis (Vista MPX) and energy dispersive X-ray spectrometer (EDX) attached to TEM.

RESULTS AND DISCUSSION

Synthesis and Characterization of MCO/P-HPC. The preparation of MCO/P-HPC is shown in Scheme 1. The P-doped hierarchical porous carbon is first synthesized using a template method coupled with an electrostatic attraction process. The SiO_2 spheres with a diameter of 400 and 20 nm, respectively, are used as hard templates. The $C_{24}H_{20}PBr$ is used as the P source. When SiO_2 spheres are added to the ethanol solution of $C_{24}H_{20}PBr$, $C_{24}H_{20}P^+$ cations combine with the OH^- anions of SiO_2 spheres by electrostatic interaction. The SiO_2@P-doped carbon is formed after pyrolysis. After the removal of SiO_2 templates, P-doped hierarchical porous carbon (P-HPC) is formed. The as-synthesized P-HPC is negatively charged because of P-doping in carbon.[17] When Co^{2+} and Mn^{2+} are added to the solution of P-HPC, they are adsorbed on the negatively charged surface of P-HPC due to the electrostatic interaction. $MnCo_2O_4$ anchored on P-HPC is produced after a hydrothermal process.

Figure 1a−c show the morphology of the as-prepared MCO/P-HPC hybrid. As can be seen, the MCO/P-HPC consists of interconnected macropores with a diameter of 300−400 nm and a wall thickness of ∼10 nm. It retains the morphology of P-HPC substrate successfully (Figure S1) except for the mesopores, which (10−20 nm in diameter) exist in the wall of macropores and between macropores of P-HPC (Figure S1b). Note that mesopores cannot be seen in MCO/P-HPC hybrid due to the uniform distribution of $MnCo_2O_4$ nanoparticles on the surface of P-HPC (Figure 1b,c). In the high-resolution TEM (HRTEM, Figure 1 d), the spacings between adjacent fringes are 0.48 and 0.29 nm, which are in conformity with the (111) and (220) lattice spacings of spinel $MnCo_2O_4$, respectively. The elemental mapping images of C, P, Co, Mn, and O are shown in Figure 1e, indicating the uniformly doping of P in carbon and uniformly distribution of Co, Mn, and O on the surface of P-HPC. The P content in P-HPC is 2.10 at. % as measured by EDX (Figure S2), which is consistent with the P content (2.13 at. %) determined from ICP-AES. The content of $MnCo_2O_4$ in the as-prepared MCO/P-HPC hybrid is determined to be about 34 wt % by the thermogravimetric analysis (TGA), as shown in Figure S3. The XRD pattern of MCO/P-HPC hybrid is shown in Figure S4a. The diffraction peaks can be well indexed to $MnCo_2O_4$ without any impurities. The wide diffraction peak of catalyst at about 2θ = 26° corresponds to the carbon substrate. The average crystallite size of $MnCo_2O_4$ is calculated to be about 8.3 nm by the Scherrer formula.

The specific surface area and porous structure of MCO/P-HPC hybrid were determined by N_2 adsorption−desorption

DOI: 10.1021/acscatal.5b00494
ACS Catal. 2015, 5, 4890−4896

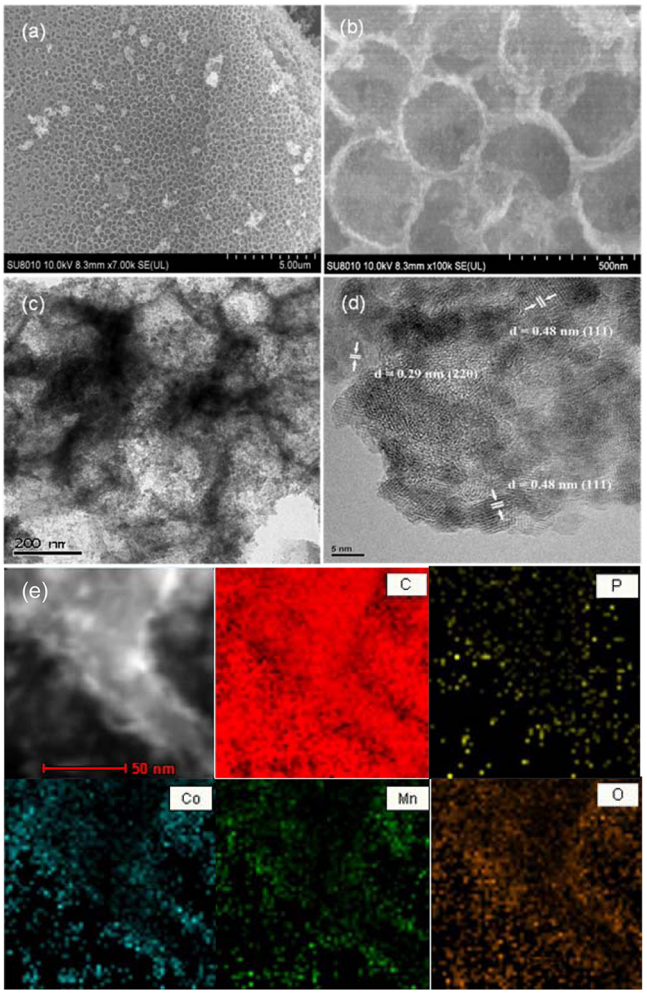

Figure 1. (a) SEM image of P-HPC; (b), (c), and (d) SEM and TEM images of MCO/P-HPC with different magnifications; (e) TEM image of MCO/P-HPC and EDX mapping images of C, P, Co, Mn, and O elements.

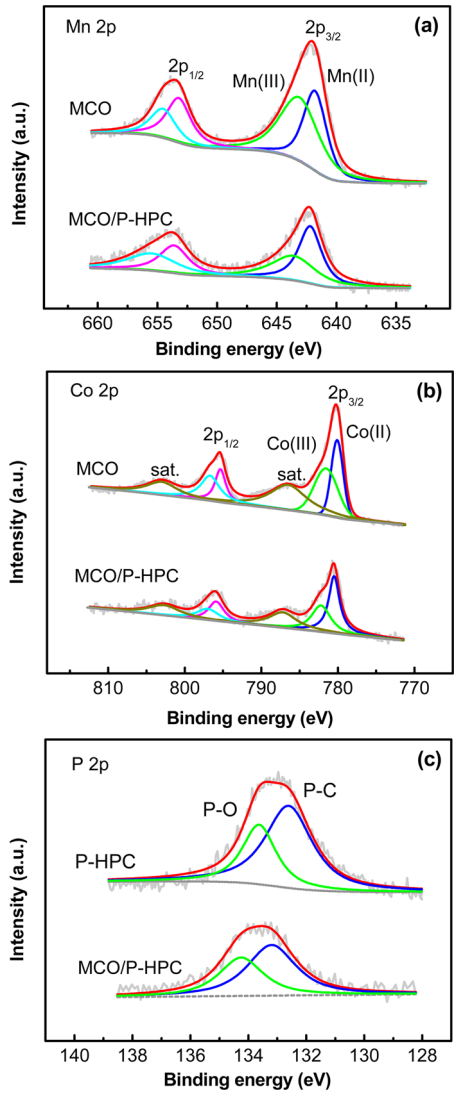

Figure 2. XPS spectra for the Mn 2p (a), Co 2p (b), and P 2p (c).

experiments, as shown in Figure S4b. A type-IV isotherm clearly demonstrates the presence of mesopores. From the pore size distribution, mesopores with a diameter of 5.6−12 nm and 20−40 nm can be clearly observed, which come from the templating of silica colloid (~20 nm in diameter) and the voids between macropores, respectively. The MCO/P-HPC possesses a surface area of 134.8 $m^2 g^{-1}$ and a total pore volume of 0.31 $cm^3 g^{-1}$. The macropores could store discharge products, and the mesopores are favorable for electrolyte penetration into the electrode and O_2 transport. This hierarchical macro-mesoporous structure also promotes the diffusion of Li^+, and the P-doped carbon network itself facilitates the transport of electron, providing an efficient triple-phase region for ORR and OER during discharge and charge process.

In order to obtain the cation oxidation state and the surface chemical composition of the MCO/P-HPC hybrid, X-ray photoelectron spectroscopy (XPS) measurements were conducted. In the high-resolution spectra of Mn 2p in MCO (Figure 2a), the asymmetric peaks of Mn $2p_{3/2}$ and Mn $2p_{1/2}$ can be fitted to two peaks, respectively. The two fitted peaks at 641.9 and 653.2 eV are ascribed to Mn^{2+}, and another two fitted two peaks at 643.3 and 654.7 eV are ascribed to Mn^{3+}.[26−28] A positive shift of 0.4 and 0.6 eV toward a high binding energy exists in the peak of Mn $2p_{3/2}$ and Mn $2p_{1/2}$, respectively, for MCO/P-HPC, as compared to MCO (Figure 2a). A positive peak shift can also be observed for the peak of Co 2p (Figure 2b). The positive shifts in Mn 2p and Co 2p indicate the electron transfer from Mn and Co atoms to the neighbor atom in the hybrid.

In the XPS spectra of P 2p in P-HPC, two deconvolved contributions at 133.9 and 132.5 eV refer to surface oxidized P species (i.e., P−O bonding) and P−C bonding (Figure 2c).[29−31] The results along with the XPS spectra of C 1s (Figure S5) reveal that P atom has been incorporated into the carbon lattice.

Remarkably, a positive shift of about 0.7 eV in the binding energy of P 2p in MCO/P-HPC with respect to P-HPC is observed, which most likely results from the chemical coupling between metal atom and oxidized phosphorus, such as the M−O−P (M = Mn, Co) bond. Note that the surface amount of P in P-HPC is 1.96 at. % as calculated from the XPS data by measuring the ratio of C 1s to P 2p intensities (integrated peak area) normalized by their respective sensitivity factors. It is very close to the bulk content obtained from the EDX (2.10 at. %) and ICP-AES (2.13 at. %). The shift of the binding energy in Co 2p, Mn 2p as well as P 2p reveals the covalent coupling between MCO and P-HPC in MCO/P-HPC. This covalent

DOI: 10.1021/acscatal.5b00494
ACS Catal. 2015, 5, 4890−4896

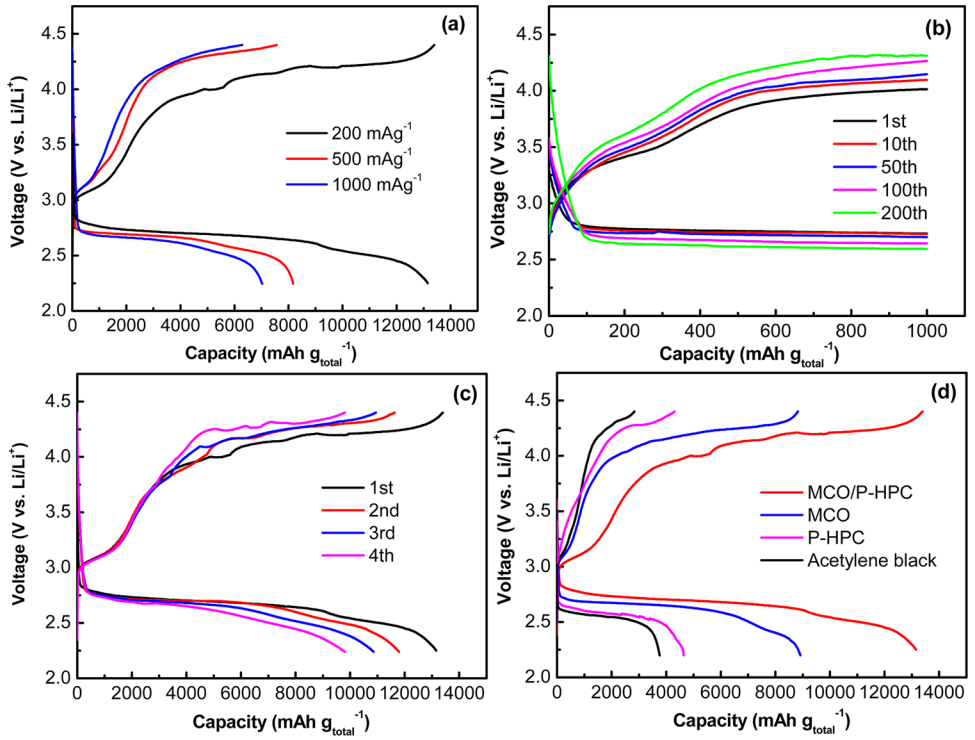

Figure 3. (a) Discharge curves of the MCO/P-HPC cathode at various current densities of 200 mA g^{-1}, 500 mA g^{-1}, and 1000 mA g^{-1}; (b) The cycling performance of MCO/P-HPC cathode at a limited depth of discharge of 1000 mAh g^{-1} and a current density of 200 mA g^{-1}; (c) Full discharge/charge curves of MCO/P- HPC between 2.2 and 4.4 V at 200 mA g^{-1} for the first four cycles. (d) The comparison between the discharge/charge capacity of MCO/P-HPC with that of MCO, P-HPC, and acetyelene black.

bonding provides pathways for charge transport through the interface and thus promotes the electrochemical catalytic activity. Furthermore, P-doping induces charge redistribution in the carbon atom and structure defects, which are favorable for O_2 adsorption and facilitate the ORR process.[26,31,32]

The above results indicate that P-doping in carbon is an effective way for the modification of carbon to be favorable for anchoring metal oxides on carbon. This process does not involve pretreatment with harsh oxidation and thus avoid the possible conductivity decreasing or the architecture of carbon support destroying.[24] Moreover, it is worth noting that optimized P-doping in carbon can increase the electrical conductivity of carbon based on our previous study.[17] When P is doped in carbon, P is positively charged, and C is negatively charged due to the smaller electronegativity of P than C. Meanwhile, the P bonded to C is partially oxidized, as confirmed by the high resolution P 2p spectrum (Figure 2c). The O atom bonded to P is also negatively charged.[33] Therefore, positively charged metal ions, such as Co^{2+} and Mn^{2+}, are facile to be absorbed on the surface of carbon due to the electrostatic interaction during the hydrothermal process (Scheme 1).

Electrochemical Performance of MCO/P-HPC. The electrocatalytic activity of MCO/P-HPC air electrode was evaluated in a Li−O_2 cell. MCO and P-HPC were also tested for comparison in which 1 M LiTFSI/TEGDME was used as the electrolyte. The current density and specific capacity are normalized to the total mass of catalyst (MCO/P-HPC, P-HPC, MCO), binder, and carbon black (acetylene black). The weight of carbon paper is not considered in the calculation of the discharge/charge capacity because the capacity of the same Torray carbon paper alone has been reported to be very limited (90 mAh g^{-1} at most) by other researchers.[34,25] Therefore, the contribution of the carbon paper is negligible. The discharge and charge measurements were performed in the voltage between 2.2 and 4.4 V. Figure 3a shows the discharge curves of MCO/P-HPC catalysts at different current densities. At a current density of 200 mA g^{-1}, the discharge capacity is about 13150 mAh g^{-1}. With increasing current density, the discharge capacity decreases. But even at a high current density of 1000 mA g^{-1}, the discharge capacity is still about 7028 mAh g^{-1}, suggesting excellent rate capability of MCO/P-HPC catalysts.

As shown in Figure 3b, the MCO/P-HPC hybrid catalysts exhibit excellent cycling stability with a cutoff capacity of 1000 mAh g^{-1} at a current density of 200 mA g^{-1}. In the first cycle, the discharge platform is about 2.75 V, and charge platform is lower than 4.00 V. Note that the charge profiles of MCO/P-HPC exhibit two apparent plateaus, which is similar to previous reports.[34,35−37] The lower charge plateau corresponds to the surface delithiation of Li_2O_2 or surface nonstoichiometric $Li_{2-x}O_2$, while the higher charge plateau corresponds to the bulk oxidation of Li_2O_2.[35] With increasing cycling numbers, no severe deterioration can be seen. Even in the 200th cycle, the discharge platform is still higher than 2.60 V, and the charge platform is lower than 4.40 V. The cycling performance of MCO/P-HPC catalysts is superior to that of MCO, P-HPC, and acetylene black (Figure S6), respectively. As shown in Figure S6, in the 70th cycle, the discharge platform of MCO, P-HPC, and acetylene black are 2.52, 2.63, and 2.45 V, respectively, and the charge platform of MCO, P-HPC, and acetylene black are 4.76, 4.70, and 4.87 V, respectively. Note that the Li−O_2 batteries with MCO/P-HPC catalysts show excellent cyclability over 200 cycles, much longer than the MCO-based cathodes reported early.[12,26] The MCO/P-HPC

DOI: 10.1021/acscatal.5b00494
ACS Catal. 2015, 5, 4890−4896

cathode was also tested by full charge/discharge between 2.2 and 4.4 V, as shown in Figure 3c. The initial discharge capacity reaches about 13 150 mA g^{-1} and it is still about 9803 mA g^{-1} in the fourth cycle. When the mass of discharge products Li_2O_2 is included, the initial discharge capacity is about 1070 mAh g^{-1}, which is close to the theoretical capacity of Li−O_2 battery (1165 mAh g^{-1}). Meanwhile, the Coulombic efficiency of the MCO/P-HPC cathode is almost 100% at the first four cycles (Figure S7).

The comparison between the charge/discharge capacity of MCO/P-HPC with that of MCO, P-HPC, and acetylene black (Figure 3d) clearly shows that the capacity of the former is much higher than that of MCO and P-HPC as well as that of acetylene black. Note that P-doped carbon delivers higher discharge capacity (4626 mAh g^{-1}) and charge capacity (4259 mAh g^{-1}) than acetylene black (Figure 3d), which is similar to the effect of S-doping in increasing the discharge (4300 mAh g^{-1}) and charge capacity (4100 mAh g^{-1}) of carbon reported elsewhere.[38,39] It is worth mentioning that the discharge platform of MCO (2.65 V) has been increased by 50 mV, and the charge platform (4.24 V) has been decreased by 120 mV after coupling with P-HPC. This indicates that the MCO/P-HPC hybrid efficiently decreases the overpotential of both ORR and OER and offers high catalytic activity toward these two reactions.

The high capacity, enhanced rate capability, and excellent cycling stability with low overpotential of MCO/P-HPC could be attributed to superior ORR and OER catalytic activity of strongly coupled MCO/P-HPC and the hierarchical porous structure of the MCO/P-HPC electrode, which can conserve Li_2O_2 in its macropores and transfer electrolyte, oxygen, and Li ions through its mesopores. In addition, P-HPC can provide an efficient electron conductive network. The results suggest that engineering the chemical coupling between metal oxides and carbon via P-doping is an efficient way for enhancing the activity of metal oxide electrocatalysts.

To gain insight into the discharge and charge process of MCO/P-HPC catalysts, the XRD patterns of the MCO/P-HPC cathodes discharged to 2.2 V and charged to 4.4 V were analyzed as shown in Figure 4. It can be seen from Figure 4 that

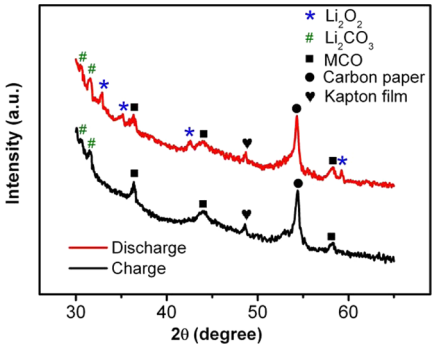

Figure 4. XRD patterns of MCO/P-HPC cathode discharged to 2.2 V and charged to 4.4 V.

the diffraction pattern of the electrode discharged to 2.2 V show that the discharged product is Li_2O_2. After it is charged to 4.4 V, the disappearance of the Li_2O_2 pattern provides the evidence of complete decomposition of discharged product Li_2O_2 (i.e., successful charging). The formation of Li_2CO_3 after discharge might result from the side reaction between Li_2O_2 and the MCO/P-HPC catalyst, the decomposition of electrolyte, or the direct reaction between oxygen anion radicals and cathode catalyst, which requires further study in the future. The accumulation of Li_2CO_3 will lead eventually to the failure of the Li−O_2 battery. The morphology of the MCO/P-HPC cathodes at different charge/discharge stages of Li−O_2 batteries was monitored by SEM image as shown in Figure 5. Figure 5a

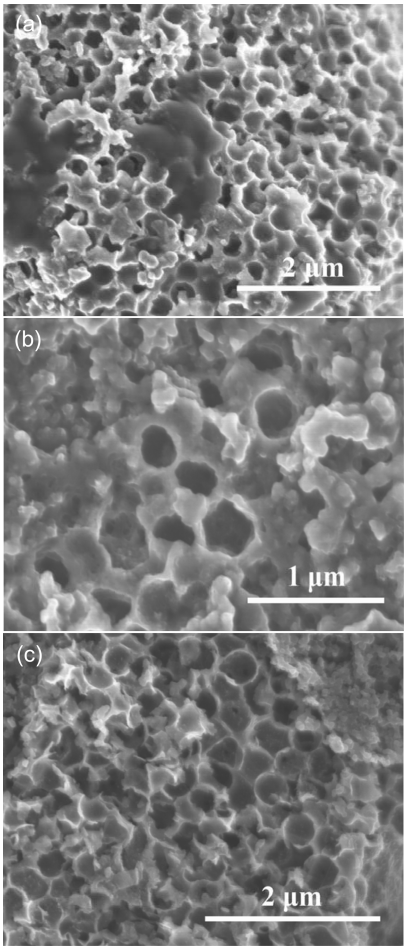

Figure 5. SEM images of MCO/P-HPC cathode discharged to a voltage of 2.6 V (a) and 2.3 V (b); (c) SEM image of MCO/P-HPC cathode recharged to 4.4 V.

shows the morphology after discharged to a voltage of 2.6 V. It can be seen that discharged product Li_2O_2 deposits uniformly onto the wall of macropores of MCO/P-HPC. The Li_2O_2 exhibits toroid-like morphology. In addition, some macropores are choked by Li_2O_2, which still can allow the transport of electrolyte and oxygen for further reactions. When the MCO/P-HPC cathode reaches a full discharge voltage of 2.3 V (Figure 5b), the thickness of the wall of macropores in MCO/P-HPC increases with respect to that discharged to 2.6 V due to the growth of Li_2O_2 on the surface of macropores. Meanwhile, almost all pores are blocked by Li_2O_2, and the discharge process ends. Disappearance of Li_2O_2 and recovery of macropores can be seen at the recharge voltage of 4.4 V, as shown in Figure 5c, which implies that discharge product Li_2O_2 decomposes almost completely (i.e., the Li_2O_2 can be reversibly formed and decomposed). This further demonstrates the high catalytic activity of MCO/P-HPC hybrid and the significant advantage

DOI: 10.1021/acscatal.5b00494
ACS Catal. 2015, 5, 4890−4896

of hierarchical porous structure of this hybrid toward both ORR and OER during the discharge and charge process.

CONCLUSIONS

In conclusion, we successfully synthesized MCO/P-HPC hybrid by growing $MnCo_2O_4$ on P-doped hierarchical porous carbon. P-doping in carbon offers an efficient strategy for anchoring metal oxides on carbon. When employed as an electrocatalyst in rechargeable Li−O_2 batteries, the MCO/P-HPC hybrid delivers a high discharge capacity of 13 150 mAh g^{-1} at a current density of 200 mA g^{-1}. The battery can sustain 200 cycles at a capacity of 1000 mAh g^{-1} with low overpotentials under 200 mA g^{-1}. The enhanced performance of Li−O_2 batteries is attributed to the chemical and electrical coupling between $MnCo_2O_4$ and P-doped carbon as well as the hierarchical macro-mesoporous structure of the MCO/P-HPC electrode. Engineering the chemical and electrical coupling between $MnCo_2O_4$ and carbon via P-doping is an effective way for enhancing the electrocatalytic activity of $MnCo_2O_4$. This work provides an alternative approach for the design of cathode electrocatalysts used in rechargeable Li−O_2 batteries.

ASSOCIATED CONTENT

Supporting Information

The Supporting Information is available free of charge on the ACS Publications website at DOI: 10.1021/acscatal.5b00494.

SEM and TEM images of P-HPC, EDX spectrum of MCO/P-HPC, TGA of MCO/P-HPC, XRD pattern, BET surface area and pore size distribution of MCO/P-HPC, high-resolution C 1s spectra of MCO/P-HPC and P-HPC, Coulombic efficiency of MCO/P-HPC for the first four cycles (PDF)

AUTHOR INFORMATION

Corresponding Author

*E-mail: yangrz@suda.edu.cn. Tel: +86-512-65221519.

Notes

The authors declare no competing financial interest.

ACKNOWLEDGMENTS

This work is supported by National Natural Science Foundation of China (Nos. 51272167 and 21206101).

REFERENCES

(1) Bruce, P. G.; Freunberger, S. A.; Hardwick, L. J.; Tarascon, J. M. *Nat. Mater.* **2012**, *11*, 19−29.
(2) Abraham, K. M.; Jiang, Z. *J. Electrochem. Soc.* **1996**, *143*, 1−5.
(3) Lee, J. S.; Kim, S. T.; Cao, R.; Choi, N. S.; Liu, M.; Lee, K. T.; Cho, J. *Adv. Energy Mater.* **2011**, *1*, 34−50.
(4) Wang, Z. L.; Xu, D.; Xu, J. J.; Zhang, L. L.; Zhang, X. B. *Adv. Funct. Mater.* **2012**, *22*, 3699−3705.
(5) Peng, Z. Q.; Freunberger, S. A.; Chen, Y. H.; Bruce, P. G. *Science* **2012**, *337*, 563−566.
(6) Yoo, E.; Zhou, H. *ACS Nano* **2011**, *5*, 3020−3026.
(7) Zhang, S. S.; Foster, D.; Read, J. *J. Power Sources* **2010**, *195*, 1235−1240.
(8) Zhou, W.; Zhang, H. Z.; Nie, H. J.; Ma, Y. W.; Zhang, Y. N.; Zhang, H. M. *ACS Appl. Mater. Interfaces* **2015**, *7*, 3389−3397.
(9) Shang, C. Q.; Dong, S. M.; Hu, P.; Guan, J.; Xiao, D. D.; Chen, X.; Zhang, L. X.; Gu, L.; Cui, G. L.; Chen, L. Q. *Sci. Rep.* **2015**, *5*, 8335−8341.
(10) Zhang, L. X.; Zhang, S. L.; Zhang, K. J.; Xu, G. J.; He, X.; Dong, S. M.; Liu, Z. H.; Huang, C. S.; Gu, L.; Cui, G. L. *Chem. Commun.* **2013**, *49*, 3540−3542.
(11) Sun, B.; Zhang, J. Q.; Munroe, P.; Ahn, H.-J.; Wang, G. X. *Electrochem. Commun.* **2013**, *31*, 88−91.
(12) Wang, H. L.; Yang, Y.; Liang, Y. Y.; Zheng, G. Y.; Li, Y. G.; Cui, Y.; Dai, H. J. *Energy Environ. Sci.* **2012**, *5*, 7931−7935.
(13) Lee, D. U.; Kim, B. J.; Chen, Z. W. *J. Mater. Chem. A* **2013**, *1*, 4754−4762.
(14) Wang, L.; Zhao, X.; Lu, Y. H.; Xu, M. W.; Zhang, D. W.; Ruoff, R. S.; Stevenson, K. J.; Goodenough, J. B. *J. Electrochem. Soc.* **2011**, *158*, A1379−A1382.
(15) Liang, Y. Y.; Li, Y. G.; Wang, H. L.; Dai, H. J. *J. Am. Chem. Soc.* **2013**, *135*, 2013−2036.
(16) Yang, D. S.; Bhattacharjya, D.; Inamdar, S.; Park, J.; Yu, J. S. *J. Am. Chem. Soc.* **2012**, *134*, 16127−16130.
(17) Zhang, M.; Dai, L. M. *Nano Energy* **2012**, *1*, 514−517.
(18) Liu, Z. W.; Peng, F.; Wang, H. J.; Yu, H.; Zheng, W. X.; Yang, J. *Angew. Chem., Int. Ed.* **2011**, *50*, 3257−3261.
(19) Wu, J.; Jin, C.; Yang, Z. R.; Tian, J. H.; Yang, R. Z. *Carbon* **2015**, *82*, 562−571.
(20) Guo, Z. Y.; Zhou, D. D.; Dong, X. L.; Qiu, Z. J.; Wang, Y. G.; Xia, Y. Y. *Adv. Mater.* **2013**, *25*, 5668−5672.
(21) Zhang, Z.; Bao, J.; He, C.; Chen, Y. N.; Wei, J. P.; Zhou, Z. *Adv. Funct. Mater.* **2014**, *24*, 6826−6833.
(22) Xu, J. J.; Wang, Z. L.; Xu, D.; Meng, F. Z.; Zhang, X. B. *Energy Environ. Sci.* **2014**, *7*, 2213−2219.
(23) Liu, S. Y.; Zhu, Y. G.; Xie, J.; Huo, Y.; Yang, H. Y.; Zhu, T. J.; Cao, G. S.; Zhao, Z. B.; Zhang, S. C. *Adv. Energy Mater.* **2014**, *4*, 1301960.
(24) Lim, H. D.; Song, H.; Kim, J.; Gwon, H.; Bae, Y.; Park, K. Y.; Hong, J.; Kim, H.; Kim, T.; Kim, Y. H.; Lepro, X.; Ovalle-Robles, R.; Baughman, R. H.; Kang, K. *Angew. Chem., Int. Ed.* **2014**, *53*, 3926−3931.
(25) Xu, J. J.; Wang, Z. L.; Xu, D.; Zhang, L. L.; Zhang, X. B. *Nat. Commun.* **2013**, *4*, Article no. 2438.
(26) Ge, X. M.; Liu, Y. Y.; Thomas Goh, F. W.; Andy Hor, T. S.; Zong, Y.; Xiao, P.; Zhang, Z.; Lim, S. H.; Li, B.; Wang, X. Z.; Liu, L. *ACS Appl. Mater. Interfaces* **2014**, *6*, 12684−12691.
(27) Tang, Q.; Jiang, L. H.; Liu, J.; Wang, S. L.; Sun, G. Q. *ACS Catal.* **2014**, *4*, 457−463.
(28) Ma, S. C.; Sun, L. Q.; Cong, L. N.; Gao, X. G.; Yao, C.; Guo, X.; Tai, L. H.; Mei, P.; Zeng, Y. P.; Xie, H. M.; Wang, R. S. *J. Phys. Chem. C* **2013**, *117*, 25890−25897.
(29) Wu, J.; Yang, Z. R.; Li, X. W.; Sun, Q. J.; Jin, C.; Strasser, P.; Yang, R. Z. *J. Mater. Chem. A* **2013**, *1*, 9889−9896.
(30) Paraknowitsch, J. P.; Zhang, Y. J.; Wienert, B.; Thomas, A. *Chem. Commun.* **2013**, *49*, 1208−1210.
(31) Wu, J.; Yang, Z. R.; Wang, Z. J.; Sun, Q. J.; Yang, R. Z. *Electrochem. Commun.* **2014**, *42*, 46−49.
(32) Choi, C. H.; Park, S. H.; Woo, S. I. *ACS Nano* **2012**, *6*, 7084−7091.
(33) Li, R.; Wei, Z. D.; Gou, X. L.; Xu, W. *RSC Adv.* **2013**, *3*, 9978−9984.
(34) Jung, H.-G.; Hassoun, J.; Park, J.-B.; Sun, Y.-K.; Scrosati, B. *Nat. Chem.* **2012**, *4*, 579−585.
(35) Gallant, B. M.; Kwabi, D. G.; Mitchell, R. R.; Zhou, J. G.; Thompson, C. V.; Shao-Horn, Yang. *Energy Environ. Sci.* **2013**, *6*, 2518−2528.
(36) Chen, W.; Lai, Y. Q.; Zhang, Z. A.; Gan, Y. Q.; Jiang, S. F.; Li, J. *J. Mater. Chem. A* **2015**, *3*, 6447−6454.
(37) Li, J.; Zou, M.; Chen, L.; Huang, Z.; Guan, L. *J. Mater. Chem. A* **2014**, *2*, 10634−10638.
(38) Li, Y. L.; Wang, J. J.; Li, X. F.; Geng, D. S.; Li, R. Y.; Sun, X. L. *Chem. Commun.* **2011**, *47*, 9438−9440.
(39) Li, Y. L.; Wang, J. J.; Li, X. F.; Geng, D. S.; Banis, M. N.; Tang, Y. J.; Wang, D. N.; Li, R. Y.; Sham, T.-K.; Sun, X. L. *J. Mater. Chem.* **2012**, *22*, 20170−20174.

DOI: 10.1021/acscatal.5b00494
ACS Catal. 2015, 5, 4890−4896